Environmental Science and Pollution Research (2018) 25:16061–16070
https://doi.org/10.1007/s11356-018-1582-5

RESEARCH ARTICLE

Study on hydrothermal deactivation of Pt/MnO_x-CeO_2 for NO_x-assisted soot oxidation: redox property, surface nitrates, and oxygen vacancies

Hailong Zhang[1] · Shanshan Li[2] · Qingjin Lin[2] · Xi Feng[1] · Yaoqiang Chen[2] · Jianli Wang[2]

Received: 8 October 2017 / Accepted: 16 February 2018 / Published online: 28 March 2018

Abstract

The study mainly focuses on surface properties to investigate the deactivation factors of Pt/MnO_x-CeO_2 by H_2 temperature-programmed reduction, CO chemical adsorption, NO_x-temperature-programmed desorption (TPD), O_2-TPD, NO temperature-programmed oxidation, SEM, TEM, in situ diffuse reflectance infrared Fourier transform spectra, Raman, and thermogravimetric methods. The results show that there are three main factors to lead to hydrothermal deactivation of the catalyst: redox property, oxygen vacancy, and surface nitrates. The loss of oxygen vacancies decreases the generation and desorption of active oxygen and that of surface nitrates weakens the production of NO_2 and surface peroxides ($-O_2^-$). These factors greatly result in the damage of the C-NO_2-O_2 cooperative reaction.

Keywords Soot oxidation · Hydrothermal aging · Deactivation · Surface nitrates · Oxygen vacancies

Introduction

The carbon nanoparticle emissions from diesel engines are well known to be a major pollutant and the cause of adverse environment and health effects; thus, the government has made great efforts to control particulate matter (PM) emissions, such as tightening emission regulations (Imran et al. 2013; Pui et al. 2014; Durgasri et al. 2014; Wierzbicka et al. 2014). In current, an effective technology for PM control is to use diesel particulate filter (DPF) to trap soot and then reduce it during DPF regeneration. However, the temperature of soot combustion is rather high (> 550 °C) and it will lead to high fuel consumption (Darcy et al. 2007; Zheng et al. 2011). Hence, there has been an increased attention on applying catalysts to decrease the temperature of soot oxidation (Azambre et al. 2011; Liu et al. 2013; Zhang et al. 2015a, b; Zhang et al. 2016).

Due to the better oxidative property and the strong oxygen storage capacity, MnO_x-CeO_2 mixed oxides have been considered as a cheap and effective candidate for diesel soot oxidation (Liu et al. 2012; Arena 2014; Quiroz et al. 2015; Zhang et al. 2017a, b). It has been reported that MnO_x-CeO_2 catalysts can exhibit better NO_x storage capacity at low temperatures and high catalytic activity for NO oxidation into NO_2 (Wu et al. 2010a, b; Liu et al. 2012). In this way, the produced NO_2 mainly results from the decomposition of NO_x-adsorbed species (surface nitrates) (Eq. (1)) and the NO oxidation by active oxygen species (O*) (Eq. (2)).

$$-NO_3 \rightarrow NO_2 + O_2 \quad (1)$$

$$NO + O^* \rightarrow NO_2 \quad (2)$$

NO_2 as a stronger oxidant than O_2 plays an important role during soot oxidation and the addition of noble metal Pt can improve the generation of NO_2 from NO oxidation over MnO_x-CeO_2 catalysts (Liu et al. 2012; Zhang et al. 2015b). Moreover, a great improvement of redox property by Pt can apparently enhance soot oxidation activity of MnO_x-CeO_2 catalysts (Zhang et al. 2015a, b).

Responsible editor: Vítor Pais Vilar

Electronic supplementary material The online version of this article (https://doi.org/10.1007/s11356-018-1582-5) contains supplementary material, which is available to authorized users.

✉ Yaoqiang Chen
nic7501@scu.edu.cn

✉ Jianli Wang
wangjianli@scu.edu.cn

[1] College of Chemical Engineering, Sichuan University, Chengdu 610064, People's Republic of China

[2] College of Chemistry, Sichuan University, Chengdu 610064, People's Republic of China

Setiabudi's study (Setiabudi et al. 2004a, b) found that in NO_2-O_2-soot system, soot oxidation reaction is firstly triggered by NO_2 to form surface oxygen complexes (SOCs, -C(O)) and then NO_2/O_2 reacts with SOCs, finally yielding CO_x; this shows a synergistic oxidation mechanism of NO_2 and O_2 (Eqs. (3) and (4)).

$$C + NO_2 \rightarrow \text{-}C(O) + NO \quad (3)$$

$$\text{-}C(O) + NO_2/O_2 \rightarrow CO_x + NO \quad (4)$$

Jeguirim et al. (2009a, b) further found that the NO_2-O_2-C cooperation reaction can be effectively enhanced in the presence of Pt/Al_2O_3 catalyst due to high produce of NO_2. According to the reports (Setiabudi et al. 2004a, b; Zhang et al. 2017a, b), it was revealed that, based on Eqs. (5) and (6), the decomposition of surface nitrates formed on the Ce-based catalysts enhances the generation of surface peroxides ($\text{-}O_2^-$) as more active oxygen species, thereby greatly promoting soot oxidation reaction rates.

$$\text{-}NO_3 \rightarrow \text{-}O_2^- + NO \quad (5)$$

$$C + \text{-}O_2^- \rightarrow CO_2 \quad (6)$$

Besides, for MnO_x-CeO_2-containing catalysts, the presence of surface active oxygen (O*) highly enhances the oxidation of NO and soot (Wu et al. 2010a, b; Liu et al. 2012; Zhang et al. 2017a, b). The consumption of active oxygen species leads to the production of oxygen vacancies (□), thereby arousing an uptake process of oxygen from gas phase. The following Eqs. (7)–(9) illustrate that the presence of oxygen vacancies is of crucial importance to improve the availability of oxygen during soot oxidation. Thus, this makes active oxygen as a main contributor to oxidize soot (Zhang et al. 2017a, b).

$$\text{-Ce-}O^*\text{-Mn-} + NO \rightarrow \text{-Ce-□-Mn-} + NO_2 \quad (7)$$

$$\text{-Ce-}O^*\text{-Mn-} + C \rightarrow \text{-Ce-□-Mn-} + CO_2 \quad (8)$$

$$\text{-Ce-□-Mn-} + O_2 \rightarrow \text{-Ce-}O^*\text{-Mn-} \quad (9)$$

Hydrothermal stability of the catalysts for soot oxidation has been confirmed to be one of main factors that lead to the deactivation of the catalysts. Many researchers have found that thermal aging at high temperatures would arouse the severe sintering of oxide crystallites; this results in the damage of structural property and the loss of surface area and thereby the deactivation of the catalysts (Aneggi et al. 2012; Liu et al. 2012; Zhang et al. 2015a, b). In fact, soot oxidation reactions occur on the contact interface between soot and catalysts; thus, some surface properties of the catalysts are important to determine the soot oxidation activity (Zhang et al. 2015a, b). However, the effects of hydrothermal aging on surface properties of the catalysts are rarely studied at present.

In this work, MnO_x-CeO_2 mixed oxides were prepared by a co-precipitation method and 0.5 wt% Pt was loaded on the support by impregnation method to obtain Pt/MnO_x-CeO_2 catalyst. The aged sample was obtained by hydrothermal treatment at 800 °C for 10 h. This work aims to explore the influences of hydrothermal aging on redox property, surface nitrate formation, and oxygen vacancies of the catalyst. The deactivation factors for soot catalytic oxidation were also discussed in the present work.

Experimental

Catalyst preparation

MnO_x-CeO_2 mixed oxides with a Mn/Ce molar ratio of 1:4 were prepared by a co-precipitation method, using $Ce(NO_3)_3 \cdot 6H_2O$ (95% pure) and $Mn(NO_3)_2$ (50 wt%) as the precursors. These precursors were dissolved in deionized water, and then the PVA (polyvinyl alcohol) was added to the aqueous solution, eventually mixing with $NH_3 \cdot H_2O$ (chemical reagents, Beijing). The pH value was controlled at 9.0. The obtained precipitates were filtered and dried at 80 °C and then calcined in air at 600 °C for 3 h in a muffle furnace. The final sample was labeled as CM and impregnated with an aqueous solution of $Pt(NO_3)_4$ (30.50 wt%, Heraeus); the loading amount of Pt was 0.5 wt% on the support. The resulting powders were dried at 120 °C for 2 h and calcined at 500 °C for 2 h. The as-received sample as the fresh catalyst was labeled as F-Pt/CM and treated at 800 °C for 10 h in 5% H_2O/air to obtain the aged sample, which was marked as A-Pt/CM.

Catalyst characterizations

The surface redox property of the catalysts was evaluated by H_2 temperature-programmed reduction (H_2-TPR). Fifty-milligram sample was used in each measurement. The samples were firstly pretreated by 5 vol% O_2/N_2 at 400 °C for 40 min, then cooled down to room temperature (RT), and followed by turning the flow of 5 vol% H_2/N_2 into the system with a flow rate of 25 ml/min. The samples were heated from RT to 800 °C at a rate of 8 °C/min. The consumption signals of H_2 were monitored by a TCD detector.

The O_2 temperature-programmed desorption (O_2-TPD) was investigated by employing 50 mg sample in each measurement. The samples were firstly pretreated by 5 vol% O_2/N_2 at 500 °C for 10 min, then cooled down to 50 °C, and followed by turning the He flow into the system with a flow rate of 25 ml/min. The samples were heated from 50 to 800 °C at a rate of 8 °C/min. The concentration signals of the desorbed O_2 were monitored by a TCD detector.

The NO temperature-programmed oxidation (NO-TPO) tests were conducted in a fixed-bed reactor. The reaction gases including 600 ppm NO/10% O_2/N_2 were fed to the fixed-bed reactor at a flow rate of 500 ml/min. Twenty milligrams of the catalyst was firstly mixed with 80 mg SiC powder, and the mixture was then used in NO-TPO tests. The reactor temperature was heated to 650 °C at a heating rate of 10 °C/min. The effluent gases were detected on an infrared (IR) spectrometer (Thermo Scientific).

The NO_x (NO and NO_2) temperature-programmed desorption (NO_x-TPD) tests were carried out in the same fixed-bed reactor. In all tests, 50 mg sample was pretreated in 600 ppm NO/10% O_2/N_2 at a flow rate of 500 ml/min. The sample was heated to 300 °C from RT at a heating rate of 10 °C/min, then cooled down to 150 °C, and only 10% O_2/N_2 was fed through the sample until RT. Subsequently, the sample was heated to 650 °C from RT at the same heating rate to obtain the desorption profiles of NO_x in N_2 or 10% O_2/N_2 flow.

SEM was performed on a FEI Inspect F50 scanning electron microscope and operated at an accelerated voltage of 30 kV to observe the morphology of the catalysts. Before testing, the samples were sputtered with gold.

The morphology of the catalysts was analyzed by transmission electron microscopy (TEM) (Tecnai G^2 F20) with an acceleration voltage of 200 kV. The sample powders were dispersed in ethanol and then deposited over Cu grids with a holey carbon film.

The diffuse reflectance infrared Fourier transform spectra (DRIFTS) were detected by using a Nicolet 6700 spectrometer equipped with a high temperature cell and a DTGS detector. Before testing, the catalyst and KBr powder were mixed at a mass ratio of 1/10. The mixed samples were placed in a high temperature cell and pretreated in situ in N_2 flow at 500 °C for 30 min and then cooled down to RT. In the cooling process, the background spectrum of each sample was recorded at every specific temperature. Afterwards, a gas mixture of 1000 ppm NO/5% O_2/N_2 was fed to the samples at a flow rate of 40 ml/min. All the spectra were recorded at 64 scans with a resolution of 4 cm^{-1}.

CO adsorption experiments were conducted on an IR spectrometer to study the impact of hydrothermal aging on Pt loaded on the surface of MnO_x-CeO_2. Prior to each test, the sample (catalyst + KBr) was pretreated at 400 °C in 5 vol% H_2/N_2 and then cooled to 30 °C in N_2 (purity 99.999%) and the background spectrum was recorded. The IR spectra of the samples were detected in N_2 flow after CO adsorption for 15 min. CO chemisorption was used to measure the dispersion of Pt by a pulse adsorption method; the testing details can be seen in the publication (Zhang et al. 2015a, b).

To further confirm the changes in electronic property or oxygen defective sites of the catalyst after aging, the IR spectra of the H_2-reduced samples were also recorded at 400 °C. The spectra of the samples before H_2 reduction were picked in N_2 flow as backgrounds. Hereafter, the reduced samples were re-oxidized by introducing 5% O_2/N_2 into reaction cell, and then the IR spectra of the re-oxidized samples were recorded in N_2 flow.

Raman spectra of the catalysts were detected on an inVia Reflex spectrometer (Renishaw, London, England) with a YAG laser (532 nm) and an output laser power of 90 mW at room temperature.

The thermogravimetric (TG) experiments were performed on a TG analyzer (HCT-2, Beijing) to study the influence of NO adsorption or nitrate formation on the acceleration of surface oxygen species on soot-catalyst interface reactions. Firstly, soot and catalysts were mixed by loose contact at a mass ratio of 1:10; then, 5.0–6.0 mg of mixtures were used for TG tests. The temperature was raised up to 800 °C from RT at a heating rate of 10 °C/min in 10% O_2/N_2. The weight loss and DTA (differential thermal analysis) signals were recorded on the TG analyzer.

Catalytic activity measurement

Printex-U (Degussa) was used as a model soot with 25 nm of particle size and 100 m^2/g of specific surface area. The soot oxidation activities of the catalysts were detected by temperature-programmed oxidation (TPO) in a continuous flow fixed-bed reactor set in a quartz tube ($\phi = 20$ mm). The sample and soot powder were mixed at a mass ratio of 10/1 by loose contact, and then, 20 mg mixture was diluted by 80 mg SiC powder to prevent reaction runaway. The obtained samples were deposited in a mini-reactor set in an electrical furnace. The reaction gases containing 600 ppm NO, 10% O_2 and N_2 as balance gas were passed through the fixed-bed reactor at a flow rate of 500 ml/min. The reaction temperature was raised from RT up to 700 °C at a ramp rate of 10 °C/min. The outlet gas CO_2 during soot-TPO was continuously detected by a CO_x analyzer (GXH-1050E, Beijing).

Results and discussion

Soot oxidation activity

The soot conversion curves of the fresh and aged Pt/MnO_x-CeO_2 catalysts in the TPO measurements are shown in Fig. 1. It can be seen that, in the presence of NO, the fresh and aged Pt/CM catalysts show much better soot oxidation activity than those in the absence of NO. This, as reported in the literature (Wu et al. 2010a, b; Liu et al. 2012), illustrates that the presence of NO apparently enhances the catalytic oxidation of soot. In summary, there may be two reasons for the promotion of NO. Firstly, the oxidation of NO over Pt/CM can induce the generation of NO_2, which is greatly beneficial to low-temperature soot oxidation and NO_2-O_2-C cooperation

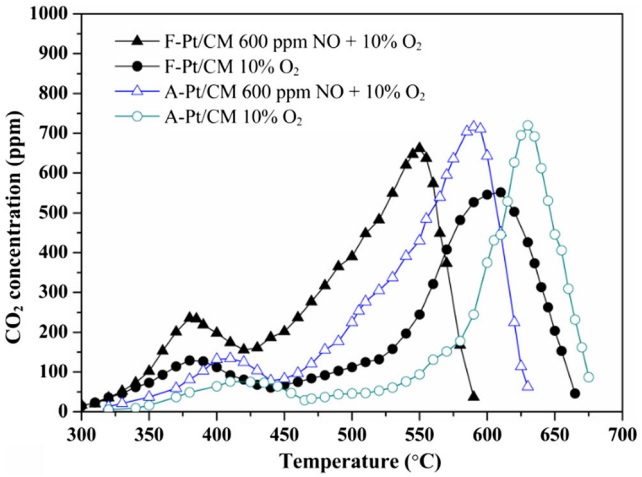

Fig. 1 Soot conversion profiles of F-Pt/CM and A-Pt/CM in O_2 and NO/O_2

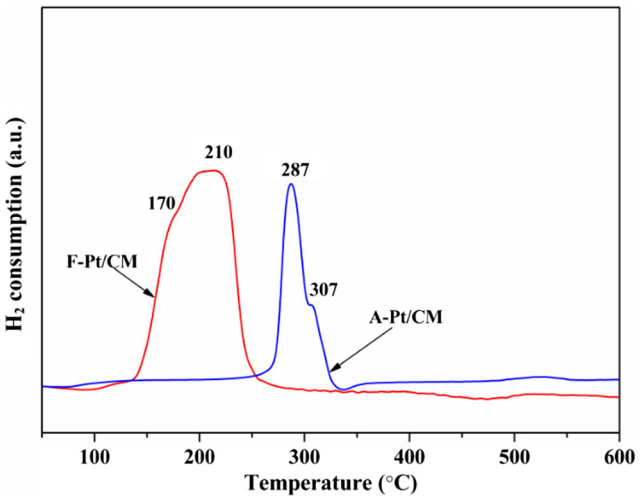

Fig. 2 H_2-TPR profiles of the fresh and aged Pt/CM catalysts

reaction (Setiabudi et al. 2004a, b; Jeguirim et al. 2009a, b, c). Secondly, the adsorption and storage of NO_x on the surface of Pt/CM would result in the formation of surface nitrates or nitrites, and the decomposition of these NO_x-intermediates might promote the generation of active oxygen species and thereby improve soot oxidation activity (Setiabudi et al. 2004a, b). Comparatively, after hydrothermal aging, in the two cases of the presence and absence of NO, the soot oxidation activity of Pt/CM clearly declines in view of the increased oxidation temperatures. Generally, hydrothermal aging at high temperatures could arouse the sintering of oxide crystalline and the decrease of specific surface area (SSA). As shown in the SEM results (see Fig. S1), a serious aggregation of particles can be observed during hydrothermal aging. These would lead to the loss of surface active sites on Pt/CM and thus weaken the generation of NO_2 and active oxygen species. These influences are rather unfavorable for NO_x-assisted soot oxidation. Fortunately, the promoting role of NO on soot oxidation activity of the aged catalyst still remains a better result in the presence of NO. In addition, it should be noticed that an apparent oxidation of soot occurs at lower temperatures (around 300–450 °C) in Fig. 1, which may be ascribed to the oxidation of partial soot with higher contact level (Zouaoui et al. 2012; Zhang et al. 2017a, b).

Redox property

The redox property of the fresh and aged Pt/CM catalysts is investigated by H_2-TPR to analyze the effects of hydrothermal aging on surface reducible species and the results are described in Fig. 2. According to the publications (Liu et al. 2012; Zhang et al. 2017a, b), for Pt/CM catalyst, the reduction peaks should be attributed to the reduction of Pt^{x+}, MnO_x, and CeO_2 species. Moreover, MnO_x-CeO_2 mixed oxides generally show a visible overlapped peak during H_2-TPR. Wang et al. (2014) reported that there are three overlapped peaks in the H_2-TPR profiles of MnO_x-CeO_2 mixed oxides, which ensues from the reduction of "isolated" Mn^{4+} species, Mn species in MnO_x-CeO_2 solid solution, and the cooperative Mn and Ce species. The strong promotion of Pt on reduction property of MnO_x-CeO_2 mixed oxides has been confirmed and makes the reduction temperatures lower (Zhang et al. 2015a, b).

In the present work, it can be clearly observed that F-Pt/CM shows a large overlapped reduction peak in Fig. 2. The peak at around 170 °C should be ascribed to the reduction of PtO_2 and partial isolated Mn species, and the overlapped peak at around 210 °C would be related to the reduction of Mn and Ce species in MnO_x-CeO_2 solid solution with the promotion of Pt. After hydrothermal aging, the catalyst shows an obviously decreased reducibility in view of the increased reduction temperature (around 287 °C). The overlapped peak appeared at 287 °C that might be attributed to the reduction of platinum oxides and fractional Mn species and that appeared at 307 °C to the reduction of the cooperative Ce and Mn species in MnO_x-CeO_2 solid solution. Moreover, it can be observed that the reduction-peak area of A-Pt/CM apparently decreases, which illustrates the loss of partial available oxygen species on the surface of the aged catalyst. This and the increased reduction temperatures should be the main factors that lead to the decrease of redox property, thus affecting the soot oxidation activity of Pt/CM.

Surface ad-NO_x species

The formation and decomposition of surface nitrates are thought of as critically important factors that can promote NO_x-assisted soot oxidation reactions. The storage of NO_x on MnO_x-CeO_2 mixed oxides results in the formation of surface nitrates, they as main ad-NO_x species would determine the desorption of NO_x. Furthermore, for Ce-based catalysts,

the decomposition of surface nitrates could promote the formation of surface active oxygen (e.g., O_2^-, O^-); this should be of crucial importance for the enhancement of soot oxidation reactions (Setiabudi et al. 2004a, b; Zhang et al. 2017a, b). To gain insight into the surface ad-NO_x species on F- and A-Pt/CM, the DRIFT spectra of the samples were studied in an IR cell and the results are shown in Fig. 3.

Based on the publications (Setiabudi et al. 2004a, b; Wu et al. 2010a, b; Zhang et al. 2017a, b), the bands of monodentate nitrates can be detected at 1040, 1237, 1290, 1440, and 1510 cm^{-1} and those of bidentate nitrates at 1040, 1270, 1310, and 1540 cm^{-1}, and the bands appearing at 1030, 1280, and 1380 cm^{-1} are ascribed to the ionic nitrates. Moreover, the chelating nitrite, nitro-compounds, and N_2O_4 species can be also found at 1205, 1410, and 1750 cm^{-1}, respectively. For the fresh sample, as shown in Fig. 3a, it can be clearly seen that the two stronger bands appear at 1205 and 1237 cm^{-1} at the testing temperature of 100 °C, with some other weaker bands such as 1040, 1310, 1380, 1410, 1440, and 1510 cm^{-1}; this illustrates that the chelating nitrites and monodentate nitrates are more easily formed at lower temperatures. And the band at 1750 cm^{-1} cannot be observed at 100 °C, which reveals that the formation of N_2O_4 is difficult at lower temperatures. With the increase of testing temperature, the bands at 1205 and 1237 cm^{-1} become very weak and other bands begin to become more apparent. This shows that the ad-NO_x species are stored mainly in the form of surface nitrates at medium temperatures (200–500 °C). It should be noted that the band assigned to ionic nitrate (1380 cm^{-1}) greatly increases in intensity at more than 400 °C, this indicates that higher temperatures are beneficial to the formation of ionic nitrates, and the result well agrees with the previous works (Wu et al. 2010a, b; Zhang et al. 2017a, b). In addition, it is found that the intensity of the bands assigned to monodentate nitrates and bidentate nitrates obviously decreases at 500 °C; this confirms that the two types of ad-NO_x species are more easily decomposed at higher temperatures.

In the case of the aged sample, as shown in Fig. 3b, it can be observed that all the bands of surface ad-NO_x species evidently decrease in the intensity at each testing temperature in comparison with Fig. 3a; it is clear that hydrothermal aging of Pt/CM seriously inhibits the formation of surface ad-NO_x species and thereby precludes the NO_x storage (see the "NO-TPO and NOx-TPD" section). From the details in Fig. 3b, it is noted that the bands at 1030, 1040, 1205, and 1750 cm^{-1} can hardly be detected at 100–500 °C, which illustrates that the storage of NO_x on Pt/CM in the form of chelating nitrite and N_2O_4 is not significant.

NO-TPO and NO_x-TPD

It is well known that NO_2 as an important oxidant plays a crucial role during both C-NO_2 reactions and C-NO_2-O_2 cooperative reactions (Wu et al. 2010a, b; Liu et al. 2012; Zhang et al. 2017a, b). Thus, NO_2 production from NO oxidation over the catalysts should be considered as an essential evaluation for soot oxidation catalysts. In this work, the NO-TPO tests were conducted in a gas flow of 600 ppm/10% O_2/N_2 to evaluate the catalytic activities of F- and A-Pt/CM for NO oxidation into NO_2; the results can be seen in Fig. 4. The fresh Pt/CM catalyst shows a better oxidation activity for NO oxidation in the wider temperature range from around 250 to 650 °C, with an onset temperature of about 100 °C and a maximal rate temperature of around 440 °C. However, the aged sample exhibits a remarkably poor activity for NO oxidation in view of higher onset temperature (around 170 °C) and higher maximal rate temperature (around 490 °C). And the amount of NO_2 production over the catalyst greatly decreases after hydrothermal aging. These results illustrate that hydrothermal aging apparently affects the NO oxidation activity inversely, thereby weakening the NO-assisted soot oxidation activity.

MnO_x-CeO_2 mixed oxides possess an excellent NO_x storage capacity, and the NO_x species are stored especially in form

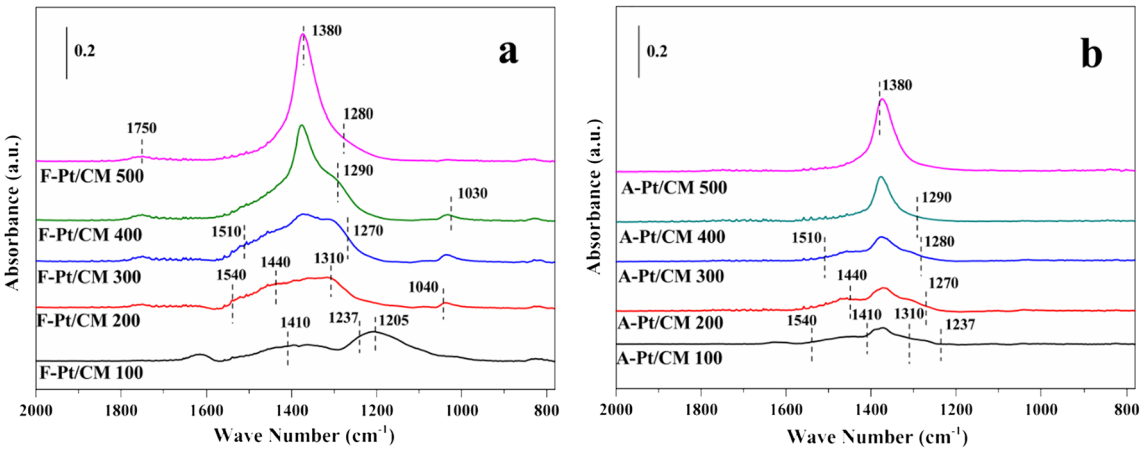

Fig. 3 DRIFTS of the fresh (**a**) and aged (**b**) samples exposed to 1000 ppm NO/5% O_2/N_2 at different temperatures

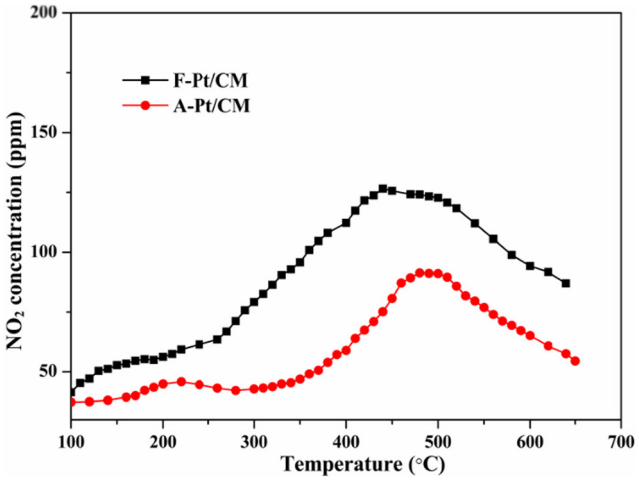

Fig. 4 NO-TPO profiles of the fresh and aged samples

of nitrates on the surface of the catalyst; this storage behavior would play an important role in NO_x-assisted soot oxidation reactions. The NO_x desorption experiments were carried out by means of TPD to investigate the NO_x storage capacity of the fresh and aged Pt/CM catalysts and the results are shown in Fig. 5. Previous to the desorption tests, the samples were purged in 10% O_2/N_2 during a cooling process from 150 °C to RT, so the NO physical adsorption on the catalyst is hardly considered here.

Figure 5a, b separately shows the NO and NO_2 desorption profiles of the samples in N_2 or 10% O_2/N_2. In N_2 gas flow, the fresh catalyst displays a larger NO desorption peak in the temperature range of 200–600 °C, while the aged sample only shows a visibly small desorption peak at around 470 °C. It can be seen in Fig. 5b that F-Pt/CM shows a weak production of NO_2 (< 5 ppm) at 250–400 °C and almost no NO_2 production is observed for the aged catalyst in N_2. However, when the desorption tests were conducted in 10% O_2/N_2, the amount of NO desorption on F-Pt/CM clearly decreases (Fig. 5a) and the NO_2 production greatly increases (Fig. 5b) at the same time. This may confirm that the desorbed NO can be oxidized into NO_2 in the presence of O_2. But, as shown in Fig. 5, this oxidation behavior of NO cannot be apparently shown in the aged catalyst, which is related to the loss of surface active oxygen and the decreased NO_x storage capacity. As mentioned in the previous sections, the storage of NO_x on MnO_x-CeO_2 mixed oxides results in the formation of surface nitrates, they as main ad-NO_x species would determine the desorption of NO_x. Thus, the NO_x desorption result well agrees with the formation of surface nitrates on the catalysts. The influences of hydrothermal aging on NO_x desorption capacity are mainly attributed to the inhibition in forming surface nitrates.

In addition, it is noted that the NO_2 production from surface nitrate decomposition in N_2 flow cannot be obviously observed in Fig. 4b. In fact, based on the previous DRIFTS results, the adsorption of NO in 10% O_2/N_2 on Pt/CM results in the formation of surface nitrates such as monodentate/bidentate nitrates and ionic nitrates, and their decomposition would lead to the production of NO_2 during the TPD (Wu et al. 2010a, b). Moreover, the formation of surface nitrites on MnO_x-CeO_2 mixed oxides is difficult at medium-high temperatures. Therefore, the desorption of partial NO should be attributed to the thermodynamic-driven decomposition of NO_2 generated from nitrate decomposition. On the other hand, NO_2 as a strong oxidizing agent can react with the reducible metal sites to form NO during the TPD tests (Atribak et al. 2009). In the publication (Setiabudi et al. 2004a, b), it was reported that the decomposition of surface nitrates would lead to the production of NO and surface peroxides ($-O_2^-$). Thus, the decomposition of surface nitrates from NO_x adsorption on Pt/CM may be one route of the production of NO and surface active oxygen. The formation and decomposition reactions of surface nitrates may be postulated in Fig. S2 (see the Supporting Information). Based on the discussion above, for

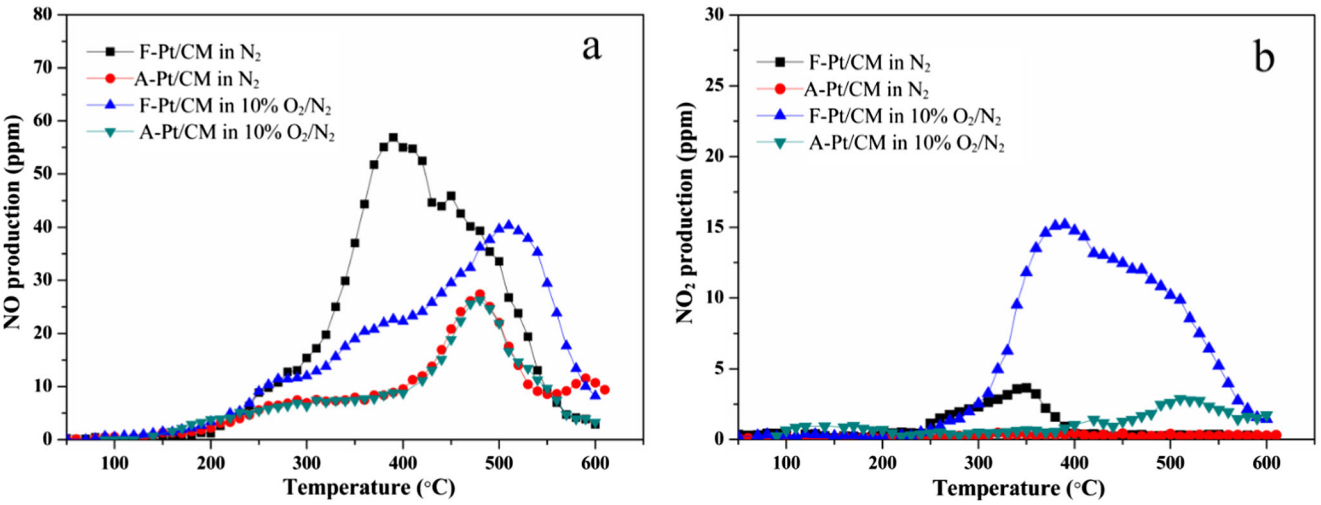

Fig. 5 **a** NO- and **b** NO_2-TPD profiles of the fresh and aged Pt/CM

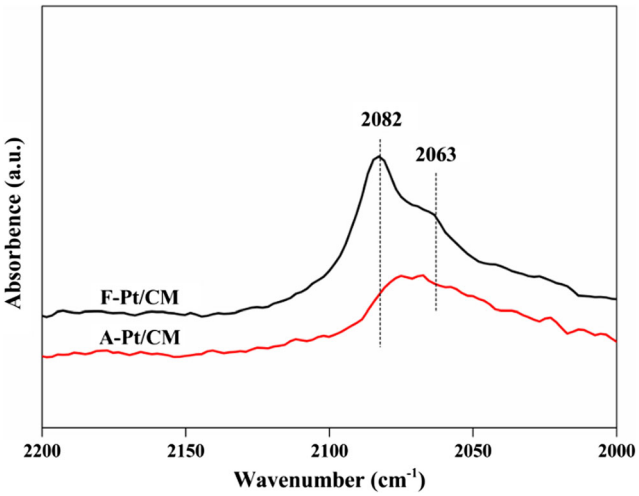

Fig. 6 IR spectra of CO adsorption on F- and A-Pt/CM

the aged sample, the weakened formation of surface nitrates decreases the production of NO_2 and surface active oxygen (O_2^-), which is very unfavorable for NO_x-assisted soot oxidation.

CO adsorption

The Pt loaded on the surface of MnO_x-CeO_2 mixed oxides plays an important role on promoting the redox property and NO oxidation into NO_2. However, thermal aging would lead to the sintering of Pt and the collapse of pore structure might arouse the encapsulation of Pt by the support. CO chemisorption is a common method that is used for the measurement of Pt dispersion. Figure 6 shows the IR spectra of CO adsorption on F- and A-Pt/CM at 30 °C. Before the CO adsorption, a pretreating process was conducted at 400 °C in 5% H_2/N_2 flow for 30 min. According to the results in Fig. 6, it can be observed that two overlapped bands appear at 2063 and 2082 cm^{-1}, which should be assigned to the linear adsorption of CO on Pt^0 (Liu et al. 2012). The fresh sample shows a stronger band intensity; this may signify a better dispersion of Pt on the support surface (14.1%, pulse adsorption). Otherwise, after hydrothermal aging, the intensity in CO adsorption bands obviously decreases, this leads to a visibly decreased dispersion of Pt (1.7%) and proves a severe sintering of Pt during hydrothermal aging. This result correlates well with TEM results (Fig. 7), a remarkable Pt particle growth on the catalyst can be observed after aging. Moreover, it can be seen that the bands of aged catalyst shift to lower wavenumber; it appears that reduction of Pt occurred, which may result from an aggregation of Pt and a loss of the interaction between Pt and the support. In the previous H_2-TPR and NO-TPO results, the aged sample shows poor reduction ability and NO oxidation activity, one reason would be ascribed to the loss of Pt active sites after thermal sintering of the catalyst.

Surface oxygen vacancies

Ceria oxides are an important material which is used for heterogeneous catalysis due to an easy production of oxygen vacancies or structural defects through the Ce^{4+}/Ce^{3+} cycle. When CeO_2 is reduced by H_2 at moderate temperatures, the non-stoichiometric CeO_x ($1.5 < x < 2$) oxides easily form, which would result in the formation of oxygen atomic point defects (Körner et al. 1989; Binet et al. 1999). In fact, forming O-defect sites more easily occurs on the surface of ceria (Sayle et al. 1992), and the surface reduction of ceria might induce the production of the bulk defects (Fallah et al. 1994). The delocalization or transition of the electrons surrounding the vacant sites would arouse a semiconductive property (Bozon-Verduraz and Bensalem 1994; Conesa 1995). These phenomenons are also shown in MnO_x-CeO_2 mixed oxides; thus, the surface electronic property of Pt/CM can be observed in IR spectra by the electronic adsorption.

Prior to IR tests, the samples were pretreated at 400 °C in pure N_2; then, the IR spectrum was recorded as background spectrum. The reduced samples were obtained by introducing 5% H_2/N_2 into the IR cell at the same temperature and then

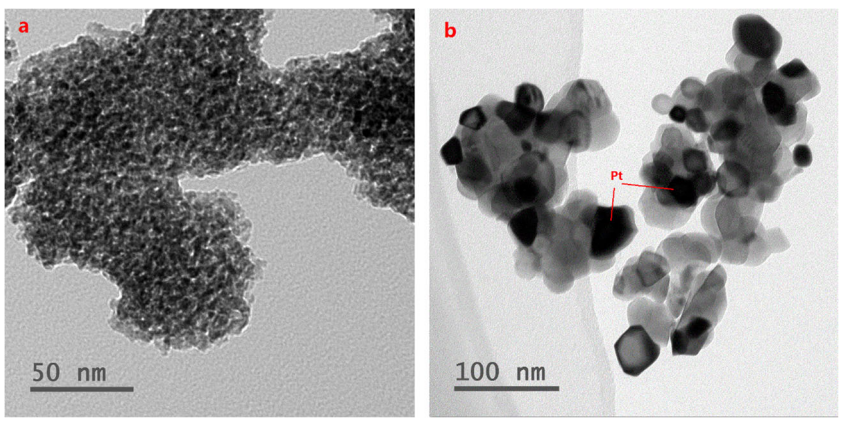

Fig. 7 TEM images of the fresh (**a**) and aged (**b**) Pt/CM

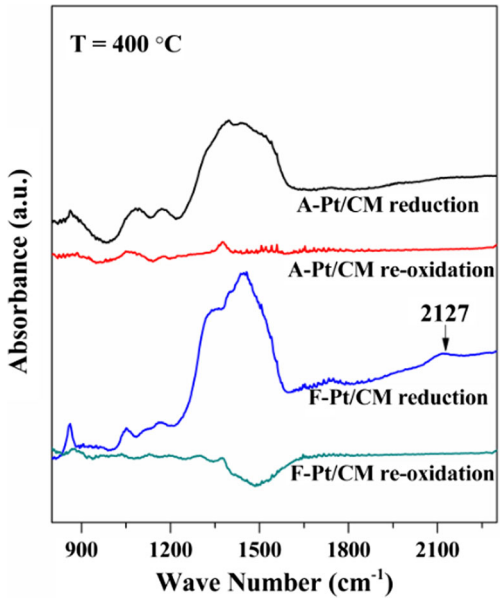

Fig. 8 IR spectra of the fresh and aged Pt/CM after reduction by H_2 and re-oxidation by O_2 at 400 °C

their IR spectra were collected. As shown in Fig. 8, for the fresh sample, it can be clearly observed that a visible band appears at the range of 1200–1600 cm^{-1}, following some weak bands at 800–1200 and 2127 cm^{-1}; these should be related to the behaviors of electrons around O-vacancies on the surface of the catalyst. Furthermore, the appearance of the band at 2127 cm^{-1}, which is assigned to the electronic transition of subsurface or bulk defective sites (Binet et al. 1999), indicates an influence of surface reduction on subsurface or bulk oxygen vacancies. By comparison, the aged sample shows a decreased IR spectrum intensity at the whole wavenumber range, which reveals a weaker surface electronic property and thereby the loss of oxygen vacancies. In essence, the result also illustrates that the sintering of the sample during hydrothermal aging might inhibit the formation of surface O-vacancies in redox process, which may be an crucial factor that affects the reduction ability of Pt/CM. Additionally, the band at 2127 cm^{-1} is not almost seen in the IR spectrum of the aged sample; this indicates that it may be difficult to form oxygen defects in the subsurface or bulk and also confirms a weakened mobility of oxygen from the bulk to surface during the reduction. After H_2 reduction, the samples were re-oxidized by the exposure in 5% O_2/N_2 and then their IR spectra were recorded. In Fig. 8, it can be observed that all the bands disappear after re-oxidation, which demonstrates the presence of the oxidized state and the loss of surface electronic property. It should be noted that there is an obvious down-band appearing at around 1500 cm^{-1} after the re-oxidation of F-Pt/CM; one possible explanation is that the reduction activates the formation of more defective sites in surface or bulk and thereby the reduced sample can take in more gas-phase oxygen to the O-vacancies during oxidizing process.

The Raman spectroscopy is also a common method to confirm the formation of the oxygen vacancies in Ce-based oxides. As reported in the publications (Taniguchi et al. 2009; Andriopoulou et al. 2017), the extent of deformations and defects in Ce-based oxides could be evaluated by a ratio of I_D/I_{F2g} or a relative intensity of I_D, where I_D is the maximum intensity of the defect band centered at ~ 600 cm^{-1} and I_{F2g} is that of F_{2g} mode that is assigned to the symmetric O-Ce-O stretching vibration. The increase of the ratio indicates an increase in concentration of O-vacancies. Thus, in order to confirm the effect of hydrothermal aging on oxygen vacancies in the catalysts, the Raman spectra of the fresh and aged Pt/CM were recorded and the results are shown in Fig. 9. The band of F_{2g} mode shifts to higher wavenumber (473 cm^{-1}) from 448 cm^{-1} after aging, which reveals the separation of Mn-Ce solid solution phases (Zhang et al. 2015a, b). It can be also seen that the ratio of I_D/I_{F2g} visibly decreases to 0.32 from 0.63 after aging, which, as same as the previous IR results, also illustrates a loss of oxygen vacancies in the catalyst.

In fact, the loss of surface O-vacancies not only leads to the decrease of surface active oxygen but also seriously affects the mobility of oxygen, thereby influencing the desorption property of oxygen (see Fig. S3). The mobility and desorption of oxygen should be considered to be very significant on the study of soot oxidation activity, since the oxygen species on the catalysts need to be desorbed and reach soot surface to oxidize soot in the solid-solid-gas interface reactions (Bassou et al. 2010).

Deactivation factors

In this study, according to the C + NO_2 + O_2 reaction mechanisms (Fig. S4, see the Supporting Information) (Liu et al.

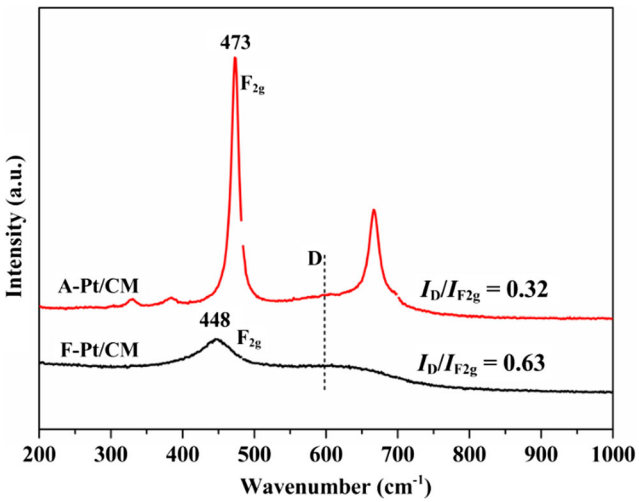

Fig. 9 Raman spectra of the fresh and aged samples. I_D/I_{F2g} is the ratio of band intensities

2012; Zhang et al. 2017a, b), there are two major factors that affect the activity of Pt/CM for soot oxidation: (1) the production of NO_2 and (2) the generation ability of active oxygen (O*) (or the storage and desorption of oxygen). These factors are closely related to the redox property, oxygen vacancies, and the formation of surface nitrates. Therefore, the following discussion about the catalytic deactivation will mainly focus on these factors.

First, in C + NO_2 reactions (Fig. S4), the production of more NO_2 as a strong oxidant from NO oxidation and nitrate decomposition on the catalysts can greatly promote the low-temperature oxidation of soot. For Pt/CM catalyst, based on the previous results, the C + NO_2 reaction activity would be affected by three factors: (1) hydrothermal aging leads to the decrease of redox property and the loss of oxygen vacancies, this directly affects the availability of active oxygen in NO oxidation reactions; (2) hydrothermal aging apparently inhibits the formation of surface nitrates, thereby decreasing the production and desorption of NO_2; and (3) the sintering and encapsulation of Pt decrease the activity of NO oxidation into NO_2.

Second, as confirmed in the previous study (Zhang et al. 2017a, b), for Pt/CM catalyst, active oxygen as a main contributor to oxidize soot despite the presence of NO_2. Based on this point, one important factor that results in the deactivation of the aged catalyst is the loss of available active oxygen, thereby weakening the C + O* → CO_x reactions. As mentioned above, the generation ability of active oxygen (O*) is a key to improve soot oxidation reaction rate. And there are two considerable factors that affect this generation ability: (1) oxygen vacancies and (2) surface nitrate formation. It has reported that the production of surface oxygen vacancies can enable the uptake ability of gas-phase oxygen and the generation of active oxygen (Katta et al. 2010; Aneggi et al. 2014; Sreeremya et al. 2015; Putla et al. 2015). Thus, the loss of oxygen vacancies on the aged catalyst (Figs. 8 and 9) is an important deactivation factor. Figure S5a (see the Supporting Information) shows a visible promoting role of surface nitrates on soot oxidation, which is ascribed not only to NO_2 but also to the surface peroxides ($-O_2^-$). The decomposition of surface nitrates enhances the generation of active oxygen (O_2^-). This promoting role cannot be seen in the aged sample (Fig. S5b), which is attributed to the loss of surface nitrates (Fig. 3).

Finally, based on the cooperative reaction, C + O_2 + O* + NO_2 → CO + CO_2 + NO + NO_2 (Zhang et al. 2017a, b), soot-NO_2 and soot-oxygen reactions are not independent but cooperative during NO_x-assisted soot oxidation (Setiabudi et al. 2004a, b; Jeguirim et al. 2009a, b). However, according to the discussion above, after hydrothermal aging, the decrease of active oxygen and NO_2 would influence these cooperative reactions. The deactivation of the catalyst would be ascribed to the damage of the cooperative role between NO_2 and oxygen.

Conclusions

The work aims to investigate the influences of hydrothermal aging on surface properties of Pt/MnO_x-CeO_2 for NO_x-assisted soot oxidation. The H_2-TPR results show that hydrothermal aging leads to the decrease of redox ability and available oxygen species, which would be attributed to the sintering of Pt and the loss of surface oxygen vacancies. Simultaneously, the loss of oxygen vacancies also seriously affects the generation ability of active oxygen, thereby decreasing the desorption of surface oxygen species. More importantly, hydrothermal aging obviously inhibits the formation of surface nitrates and limits the production of NO_2 and surface peroxides ($-O_2^-$). Thus, the loss of oxygen vacancies and surface nitrates would be crucial factors that cause the deactivation of the catalyst.

Funding information This study was financially supported by the National High Technology Research and Development Project of China (No. 2015 AA034603) and Science and Technology Project of Chengdu (No. 2015-HM01-00067-SF).

References

Andriopoulou C, Trimpalis A, Petallidou KC, Sgoura A, Efstathiou AM, Boghosian S (2017) Structural and redox properties of $Ce_{1-x}Zr_xO_{2-\delta}$ and $Ce_{0.8}Zr_{0.15}RE_{0.05}O_{2-\delta}$ (RE: La, Nd, Pr, Y) solids studied by high temperature *in situ* Raman spectroscopy. J Phys Chem C 121:7931–7943

Aneggi E, Leitenburg C, Llorca J, Trovarelli A (2012) Higher activity of diesel soot oxidation over polycrystalline ceria and ceria-zirconia solid solutions from more reactive surface planes. Catal Today 197:119–126

Aneggi E, Wiater D, Leitenburg C, Llorca J, Trovarelli A (2014) Shape-dependent activity of ceria in soot combustion. ACS Catal 4:172–181

Arena F (2014) Multipurpose composite $MnCeO_x$ catalysts for environmental applications. Catal Sci Technol 4:1890–1898

Atribak I, Azambre B, Lópeza AB, García-García A (2009) Effect of NO_x adsorption/desorption over ceria-zirconia catalysts on the catalytic combustion of model soot. Appl Catal B 92:126–137

Azambre B, Collura S, Darcy P, Trichard JM, Costa PD, García-García A, Bueno-López A (2011) Effects of a Pt/$Ce_{0.68}Zr_{0.32}O_2$ catalyst and NO_2 on the kinetics of diesel soot oxidation from thermogravimetric analyses. Fuel Process Technol 92:363–371

Bassou B, Guilhaume N, Lombaert K, Mirodatos C, Bianchi D (2010) Experimental microkinetic approach of the catalytic oxidation of diesel soot by ceria using temperature-programmed experiments. Part 1: impact and evolution of the ceria/soot contacts during soot oxidation. Energy Fuel 24:4766–4780

Binet C, Daturi M, Lavalley JC (1999) IR study of polycrystalline ceria properties in oxidised and reduced states. Catal Today 50:207–225

Bozon-Verduraz F, Bensalem A (1994) IR studies of cerium dioxide-influence of impurities and defects. J Chem Soc Faraday Trans 90: 653–657

Conesa JC (1995) Computer modeling of surfaces and defects on cerium dioxide. Surf Sci 339:337–352

Darcy P, Costa PD, Mellottée H, Trichard JM, Djéga-Mariadassou G (2007) Kinetics of catalyzed and non-catalyzed oxidation of soot from a diesel engine. Catal Today 119:252–256

Durgasri DN, Vinodkumar T, Lin FJ, Alxneit I, Reddy BM (2014) Gadolinium doped cerium oxide for soot oxidation: influence of interfacial metal-support interactions. Appl Surf Sci 314:592–598

Fallah JE, Boujana S, Dexpert H, Kiennemann A, Majerus J, Touret O, Villain F, le Normand F (1994) Redox processes on pure ceria and on Rh/CeO_2 catalyst monitored by X-ray absorption (fast acquisition mode). J Phys Chem 98:5522–5533

Imran A, Varman M, Masjuki HH, Kalam MA (2013) Review on alcohol fumigation on diesel engine: a viable alternative dual fuel technology for satisfactory engine performance and reduction of environment concerning emission. Renew Sust Energ Rev 26:739–751

Jeguirim M, Tschamber V, Brilhac JF (2009a) Kinetics of catalyzed and non-catalyzed soot oxidation with nitrogen dioxide under regeneration particle trap conditions. J Chem Technol Biotechnol 84:770–776

Jeguirim M, Tschamber V, Brilhac JF (2009b) Kinetics and mechanism of the oxidation of carbon by NO_2 in the presence of water vapor. Inc Int J Chem Kinet 41:236–244

Jeguirim M, Tschamber V, Villani K, Brilhac JF, Martens JA (2009c) Mechanistic study of carbon oxidation with NO_2 and O_2 in the presence of a Ru/Na-Y catalyst. Chem Eng Technol 32:830–834

Katta L, Sudarsanam P, Thrimurthulu G, Reddy BM (2010) Doped nanosized ceria solid solutions for low temperature soot oxidation: zirconium versus lanthanum promoters. Appl Catal B 101:101–108

Körner R, Ricken M, Nölting J, Riess I (1989) Phase transformations in reduced ceria: determination by thermal expansion measurements. J Solid State Chem 78:136–147

Liu S, Wu XD, Weng D, Li M, Lee HR (2012) Combined promoting effects of platinum and MnO_x-CeO_2 supported on alumina on NO_x-assisted soot oxidation: thermal stability and sulfur resistance. Chem Eng J 203:25–35

Liu S, Wu XD, Weng D, Li M, Fan J (2013) Sulfation of Pt/Al2O3 catalyst for soot oxidation: high utilization of NO_2 and oxidation of surface oxygenated complexes. Appl Catal B 138-139:199–211

Pui DYH, Chen SC, Zuo ZL (2014) $PM_{2.5}$ in China: measurements, sources, visibility and health effects, and mitigation. Particuology 13:1–26

Putla S, Amin MH, Reddy BM, Nafady A, Al Farhan KA, Bhargava SK (2015) MnO_x nanoparticle-dispersed CeO_2 nanocubes: a remarkable heteronanostructured system with unusual structural characteristics and superior catalytic performance. ACS Appl Mater Interfaces 7: 16525–16535

Quiroz J, Giraudon JM, Gervasini A, Dujardin C, Lancelot C, Trentesaux M, Lamonier JF (2015) Total oxidation of formaldehyde over MnO_x-CeO_2 catalysts: the effect of acid treatment. ACS Catal 5: 2260–2269

Sayle T, Parker S, Catlow RC (1992) Surface oxygen vacancy formation on CeO_2 and its role in the oxidation of carbon-monoxide. J Chem Soc Chem Commun:977–978

Setiabudi A, Chen JL, Mul G, Makkee M, Moulijin JA (2004a) CeO_2 catalysed soot oxidation: the role of active oxygen to accelerate the oxidation conversion. Appl Catal B 51:9–19

Setiabudi A, Makkee M, Moulijn JA (2004b) The role of NO_2 and O_2 in the accelerated combustion of soot in diesel exhaust gases. Appl Catal B 50:185–194

Sreeremya TS, Krishnan A, Remani KC, Patil KR, Brougham DF, Ghosh S (2015) Shape-selective oriented cerium oxide nanocrystals permit assessment of the effect of the exposed facets on catalytic activity and oxygen storage capacity. ACS Appl Mater Interfaces 7:8545–8555

Taniguchi T, Watanabe T, Sugiyama N, Subramani AK, Wagata H, Matsushita N, Yoshimura M (2009) Identifying defect in ceria-based nanocrystals by UV resonance Raman spectroscopy. J Phys Chem C 113:19789–19793

Wang XY, Ran L, Dai Y, Lu YJ, Dai QG (2014) Removal of Cl adsorbed on Mn-Ce-La solid solution catalysts during CVOC combustion. J Colloid Interface Sci 426:324–332

Wierzbicka A, Nilsson PT, Rissler J, Sallsten G, Xu YY, Pagels JH, Albin M, Österberg K, Strandberg B, Eriksson A, Bohgard M, Bergemalm-Rynell K, Gudmundsson A (2014) Detailed diesel exhaust characteristics including particle surface area and lung deposited dose for better understanding of health effects in human chamber exposure studies. Atmos Environ 86:212–219

Wu XD, Lin F, Xu HB, Weng D (2010a) Effects of adsorbed and gaseous NO_x species on catalytic oxidation of diesel soot with MnO_x-CeO_2 mixed oxides. Appl Catal B 96:101–109

Wu M, Wang XY, Dai QG, Gu YX, Li D (2010b) Low temperature catalytic combustion chlorobenzene over Mn-Ce-O/γ-Al_2O_3 mixed oxides catalyst. Catal Today 158:336–342

Zhang HL, Wang JL, Cao Y, Wang YJ, Gong MC, Chen YQ (2015a) Effect of Y on improving the thermal stability of MnO_x-CeO_2 catalysts for diesel soot oxidation. Chin J Catal 36:1333–1341

Zhang HL, Zhu Y, Wang SD, Zhao M, Gong MC, Chen YQ (2015b) Activity and thermal stability of Pt/$Ce_{0.64}Mn_{0.16}R_{0.2}O_x$ (R = Al, Zr La, or Y) for soot and NO oxidation. Fuel Process Technol 137:38–47

Zhang HL, Wang JL, Zhang YH, Jiao Y, Ren CJ, Gong MC, Chen YQ (2016) A study on H_2-TPR of Pt/$Ce_{0.27}Zr_{0.73}O_2$ and Pt/$Ce_{0.27}Zr_{0.70}La_{0.03}O_x$ for soot oxidation. Appl Surf Sci 377:48–55

Zhang HL, Hou ZY, Zhu Y, Wang JL, Chen YQ (2017a) Sulfur deactivation mechanism of Pt/MnO_x-CeO_2 for soot oxidation: surface property study. Appl Surf Sci 396:560–565

Zhang HL, Yuan SD, Wang JL, Gong MC, Chen YQ (2017b) Effects of contact model and NO_x on soot oxidation activity over Pt/MnO_x-CeO_2 and the reaction mechanisms. Chem Eng J 327:1066–1076

Zheng MG, Gao H, Zhu XH (2011) Research on developing DPF blow-back heating regeneration device. Procedia Eng 16:661–666

Zouaoui N, Issa M, Kehrli D, Jeguirim M (2012) CeO_2 catalytic activity for soot oxidation under NO/O_2 in loose and tight contact. Catal Today 189:65–69